

Retrofitting Shear Critical Beams using Ultra High Performance Fibre Reinforced Concrete (UHPFRC)

S. Bandara and K.K. Wijesundara

Abstract: Ultra High-Performance Fiber Reinforced Concrete (UHPFRC) is a cementitious composite that exhibits superior mechanical properties, durability, fire resistance, abrasion resistance, and chloride penetration. The enhanced performance of UHPFRC is attributed to the presence of high-strength steel fibers. Therefore, UHPFRC is widely used in structural retrofitting and rehabilitation works to improve the load carrying capacity of deteriorated structural members. This paper investigates the behaviour of UHPFRC retrofitted shear critical reinforced concrete beams. Numerical models were developed to simulate how the load-carrying capacity of UHPFRC retrofitted shear critical beams is influenced by factors such as jacket configuration, jacket thickness, and jacket length along the beam. Numerical models were validated using pre-existing experimental results. A modified Concrete Damage Plasticity (CDP) model was employed to simulate the material behaviour of UHPFRC. The validated numerical model was employed to perform parametric studies to examine the behaviour of UHPFRC retrofitted beams. It was observed that the modified CDP model effectively predicted the UHPFRC behaviour. Further, the results indicated that the application of UHPFRC retrofitting converted the brittle shear failure of shear-critical reinforced concrete beams into flexure failure. Moreover, the load carrying capacity of retrofitted beams increased with the retrofitted UHPFRC jacket thickness.


Keywords: Retrofitting, UHPFRC, Jacketing, Flexural strength, Concrete damage, Plasticity

1. Introduction


Ultra High-Performance Fiber-Reinforced Concrete (UHPFRC) stands as a cement-based advanced construction material that combines cement with fine steel or synthetic fibers, resulting in remarkable strength, ductility, and durability. With superior compressive strength, minimal water content, and exceptional flexural strength, it outperforms conventional concrete [1]. UHPFRC delivers outstanding performance by exhibiting extremely low permeability. This quality translates to minimal penetration of detrimental substances, including water and chlorides [2]. With resilience to environmental stresses, UHPFRC proves ideal for challenging engineering endeavours that demand long-lasting endurance. Due to the dense matrix of UHPFRC and low ingress of water and chlorides, reinforcement corrosion is kept minimum prolonging the service life of UHPFRC members [3]. Its noteworthy capacity to withstand bending and tensile forces makes it an unparalleled performer, establishing it as a preferred choice in civil engineering for its robustness and adaptability. In general, UHPFRC exhibits compressive strengths exceeding 150 MPa, tensile strengths greater than 10 MPa and exceptional tensile strain hardening behaviour [1].

The primary distinction in the composition between conventional reinforced concrete and UHPFRC lies in the inclusion of steel fibers in UHPFRC and the absence of coarse aggregates [4]. The elevated cement content in UHPFRC contributes to increased costs, prompting the utilization of supplementary cementitious materials such as silica fume in the mix. These materials are utilized to partially substitute Portland cement, addressing cost concerns while upholding performance standards. Superplasticizers are used in the mix of UHPFRC to maintain workability while preserving a lower water-to-binder ratio. Further, to enhance the workability, reduce the cement content and to control shrinkage, filler materials like crushed quartz find extensive use in the mix of UHPFRC [5].

Eng. (Dr.) S. Bandara, AMIE(SL), B.Sc. Eng. (Hons.) (Peradeniya), Ph.D. (Swinburne), Department of Civil Engineering, University of Peradeniya.
Email: sahan@eng.pdn.ac.lk

 <https://orcid.org/0000-0002-9090-7057>

Eng. (Prof.) K. K. Wijesundara, AMIE(SL), B.Sc. Eng. (Hons.) (Peradeniya), M.Sc. (Pavia), Ph.D. (Pavia), Professor of Civil Engineering, Department of Civil Engineering, University of Peradeniya.
Email: kushanw@pdn.ac.lk

 <https://orcid.org/0000-0002-4174-8707>



In recent times, considerable attention has been directed towards reinforced concrete structures exposed to challenging environmental conditions, resulting in premature deterioration. In the Sri Lankan context, this issue is notably evident in the school building system, particularly in coastal regions. Figure 1 illustrates photos of deteriorated reinforced concrete (RC) columns and slabs in Sri Lankan school buildings located in the coastal region. It can be observed that the reinforcement is exposed to an atmosphere containing chlorides, leading to a significant compromise in the structural integrity of these buildings. Apart from experiencing premature deterioration, certain structures undergo increased mechanical loads that surpass the originally intended design values. This occurs as a result of modifications in usage to meet evolving needs. Furthermore, discrepancies in design and inaccuracies in construction underscore the necessity for structural retrofitting of RC members. Structural retrofitting is essential to guarantee the safety and functionality of deteriorated concrete structures.

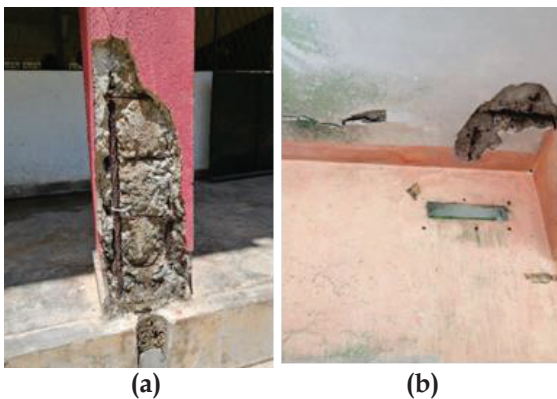


Figure 1 - Deteriorated RC elements in Sri Lankan school buildings (a) columns (b) slabs

The preference for structural retrofitting has gained prominence over demolition and rebuilding, primarily driven by considerations of economic viability and sustainability. Dominant techniques of structural retrofitting include RC jacketing [7], steel jacketing [8], Fibre Reinforced Polymer (FRP) wrapping [9] and using laminated composite plates [10]. Each of these techniques possesses its own distinctive shortcomings and limitations. For example, the process of RC jacketing demands thicker jackets, typically exceeding 70 mm [11]. This, however, poses challenges as it impedes the architectural space and leads to an increased self-weight of the structure [11]. In contrast, external jacketing using steel and FRP

requires smaller jacket thicknesses. However, delamination is a common issue encountered in FRP retrofitting. In addition, the fire performance of steel and FRP retrofitted structural members is poor. Further, externally jacketed steel plates are susceptible to corrosion, compromising the load carrying capacity. UHPFRC jacketing can overcome most of the issues in conventional retrofitting techniques [6].

The retrofitting of structural members with UHPFRC has found widespread application in various aspects, including flexural strengthening, combined axial and flexural strengthening, shear strengthening, torsional strengthening, and enhancement of impact resistance [6]. Previous researchers have explored the retrofitting of various structural members, including beams, columns, slabs, and load-bearing walls, using UHPFRC (e.g., [6, 11]). The scope of this study is limited to the rehabilitation of RC beams. The behaviour and the failure mode of RC beams rely on span to depth ratio. Beams characterized by a higher span-to-depth ratio are prone to ductile flexural failure, while those with a lower span-to-depth ratio, referred to as deep beams, are susceptible to brittle shear failure. The flexural strengthening of RC beams using UHPFRC has been extensively researched, as evidenced by studies such as [12, 13]. However, there are limited studies on the behaviour of shear-critical beams strengthened with UHPFRC. Therefore, this study aims to explore the behaviour of UHPFRC retrofitted shear critical RC beams. Finite element models were developed to numerically investigate the effects of UHPFRC jacket thickness and jacket configuration on the improvement of the load carrying capacity of shear critical beams.

2. Numerical Simulation

ABAQUS software version 2021 was used to develop 3-dimensional solid Finite Element (FE) models to simulate the behaviour of simply supported RC beams subjected to three-point bending. The modelling process began with an initial intact RC control beam, followed by the modelling of various UHPFRC retrofitting configurations. The aim was to compare the resulting enhancements in load-carrying capacity and the changes in the failure modes with the introduction of UHPFRC jacketing to RC shear critical beams. Ensuring accurate representation of the material behaviour in FE models is essential for obtaining reliable and accurate results. The

subsections 2.1 and 2.2 briefly describe the material models and the corresponding constitutive relationships used to model concrete, conventional reinforcement and UHPFRC.

2.1 Material Models for Concrete and Reinforcement

The "Concrete Damage Plasticity model" (CDP) is well defined in ABAQUS to model concrete and it is based on a plasticity-based continuum damage model [14]. The inelastic material behaviour is characterized for tension and compression by specifying a scalar damage parameter, which serves as an internal variable to define the damage model [15]. The CDP model employs a non-associated flow rule. Micro-cracks in tension are captured with a softening branch in the stress-strain relationship whereas in compression, plastic response is generally modelled with a strain hardening followed by a softening branch. Uniaxial tensile and compressive stress-strain data are required to define the strain hardening/softening behaviour of concrete. The progression of yield (or failure) is governed by equivalent plastic strains, which are linked to failure mechanisms under both tension and compression loading [15]. In total, five parameters are necessary to define the yield function, plastic potential, and visco-plastic regularization. The ratio of initial biaxial compressive strength to initial uniaxial compressive strength, σ_{bo}/σ_{co} , and parameter k_c are two crucial parameters used to define the shape of the yield surface. The yield function can be defined as,

$$f = \frac{1}{1-\alpha}(\bar{q} - 3\alpha\bar{p} + \beta(\bar{\epsilon}^{pl})\langle\bar{\sigma}_{max}\rangle) - \gamma\langle\bar{\sigma}_{max}\rangle - \bar{\sigma}_c(\bar{\epsilon}^{pl}) \leq 0 \quad \dots(1)$$

where \bar{p} is the hydrostatic pressure based on effective stresses, \bar{q} is the effective von Mises equivalent stress, α and γ are dimensionless material constants controlled by σ_{bo}/σ_{co} and k_c , $\bar{\sigma}_{max}$ is the effective major principal stress, and $\bar{\sigma}_c$ is the effective cohesive stress in compression and $\bar{\epsilon}^{pl}$ is a function of the accumulated plastic strain.

Experimental testing can be performed to obtain stress-strain behaviour under uniaxial compression. The relationship between inelastic strain ϵ_c^{in} , total strain ϵ_c and elastic strain

ϵ_{oc}^{el} is as follows which is illustrated in Figure 2.

$$\epsilon_c^{in} = \epsilon_c - \epsilon_{oc}^{el} \quad \dots (2)$$

$$\epsilon_{oc}^{el} = \sigma_c/E_o \quad \dots (3)$$

where E_o is the undamaged (initial) elastic modulus. The plastic strain ϵ_c^{pl} can be computed from the geometry shown in Figure 2. d_c shown in Figure 2 is the damage parameter in compression and this is varied from 0 to 1. 0 represents the undamaged case whereas, 1 refers to the completely damaged case. The effective compressive stress, $\bar{\sigma}_c$, can be found in the following relationships.

$$\sigma_c = (1 - d_c)E_o(\epsilon_c - \epsilon_c^{pl}) \quad \dots (4)$$

$$\bar{\sigma}_c = \sigma_c/(1 - d_c) = E_o(\epsilon_c - \epsilon_c^{pl}) \quad \dots (5)$$

$$\epsilon_c^{pl} = \epsilon_c^{in} - \frac{d_c}{(1 - d_c)} \frac{\sigma_c}{E_o} \quad \dots (6)$$

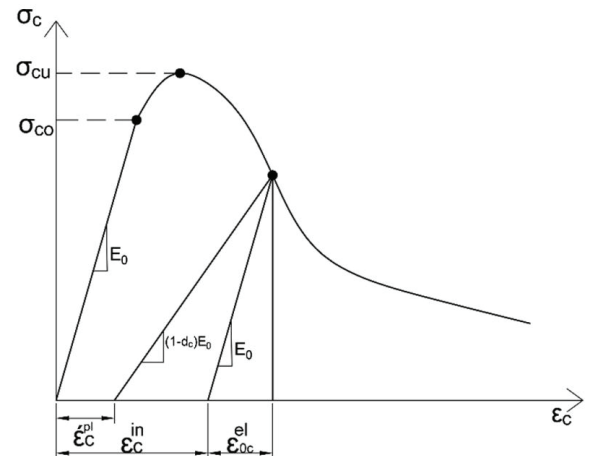


Figure 2 - Uniaxial Stress-Strain Showing Strain Components (Elastic, Plastic) and Damage [15]

Hardening and softening behaviour in tension can be characterized by obtaining the cracking strain. The tensile stress, effective tensile stress and plastic strain can be obtained similar to that of compression using Equations (4)-(6). The softening curve of concrete under tension is illustrated in Figure 3, where G_F is the fracture energy. The softening branch can be modelled as linear, bilinear, or exponential considering the results of previous studies [16]. Figure 3 shows a bilinear softening branch that follows the linear phase until cracking.

The conventional steel reinforcement was assumed to be perfectly bonded to concrete and thus, a bonded contact was employed in



numerically simulating the composite behaviour. The steel was assumed to exhibit a bilinear elastic-perfectly plastic behaviour, with identical characteristics in both tension and compression, as depicted in Figure 4, where f_y is the yield strength of steel.

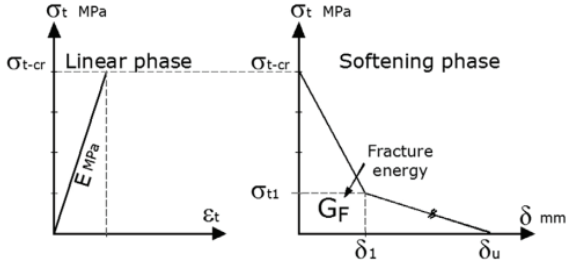


Figure 3 - Uniaxial Tensile Behaviour (Linear and Softening Phases) [15]

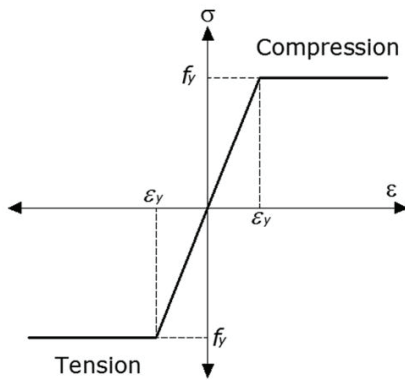


Figure 4 - Stress-Strain Behaviour for Conventional Reinforcement [15]

2.2 Material Models for UHPFRC

The material model for UHPFRC can utilize the CDP model, initially designed for normal-strength concrete and explained in the preceding section, with necessary modifications. When experimental testing provides uniaxial tensile and compressive stress-strain data, such information can be directly input into the CDP model to simulate the nonlinear behaviour of UHPFRC. Nevertheless, when experimental data is not available, uniaxial tensile and compressive stress-strain response needs to be obtained via the empirical equations derived by previous researchers [17]. These empirical equations are derived from test data. This study used the empirical equations proposed by Singh et al. [15] to model the non-linear compression response of UHPFRC, since those equations are validated with a wide array of UHPFRC test data. Further, these empirical equations have been widely used in modelling the compressive behaviour of UHPFRC elements. Empirical equations used in this study are as follows.

For $0 \leq \varepsilon \leq \varepsilon_o$

$$\sigma_c = f_c' \left[\frac{(E_o/E_{sc})(\varepsilon/\varepsilon_o) - (\varepsilon/\varepsilon_o)^2}{1 + (E_o/E_{sc} - 2)(\varepsilon/\varepsilon_o)} \right] \quad \dots(7)$$

For $\varepsilon_o \leq \varepsilon$

$$\sigma_c = \left[\frac{f_c'}{1 + 1/4 \{ (\varepsilon/\varepsilon_o) - 1 \} \{ (\varepsilon_L/\varepsilon_o) - 1 \}^{1.5}} \right] \quad \dots(8)$$

where ε_o is the strain corresponding to peak stress, E_o is the undamaged (initial) elastic modulus, E_{sc} is the secant modulus and f_c' is the peak compressive stress. The limiting strain ε_L can be found from the following equations.

$$\varepsilon_L = \varepsilon_o \left[\left(\frac{1.25 E_o}{10 E_{sc}} + \frac{4}{5} \right) + \sqrt{\left(\frac{1.25 E_o}{10 E_{sc}} + \frac{4}{5} \right)^2 + \frac{4}{5}} \right] \quad \dots(9)$$

$$\varepsilon_o = 750 (f_c')^{0.35} \times 10^{-6} \quad \dots(10)$$

$$E_o = 15050 (f_c'/10)^{1/3} \quad \dots(11)$$

$$E_{sc} = f_c'/\varepsilon_o \quad \dots(12)$$

Singh et al. [15] performed experiments to verify the performance of the aforementioned empirical equations and a good agreement was found between experimental results and the predictions. The damage parameter used in this study is defined as follows.

$$d_c = 1 - \left[\frac{\sigma_c/E_o}{0.2 \varepsilon_c^{in} + \sigma_c/E_o} \right] \quad \dots(13)$$

The tensile behaviour of UHPFRC is illustrated in Figure 5 where three distinct phases can be found such as linear elastic, strain hardening and strain softening phases. The first branch in the stress-strain curve is the linear elastic phase where stress is linearly increased without any crack formation until cracking strength. In this phase, the fibres resist the opening of micro cracks by fibre bridging. In the second phase, micro cracks are formed and fibres tend to pull out from the matrix. Cracks are distributed and widened in this phase until the tensile strength of fibres is reached. Once the tensile strength is reached, localised macro cracks form and propagate in the third phase resulting in strain softening. Fracture takes place when no more stress is transferred through the localised microcracks [11]. Cracks are distributed and widened in this phase until the tensile strength of fibres is reached. Once the tensile strength is reached, localised macro cracks form and propagate in the third phase resulting in strain softening.

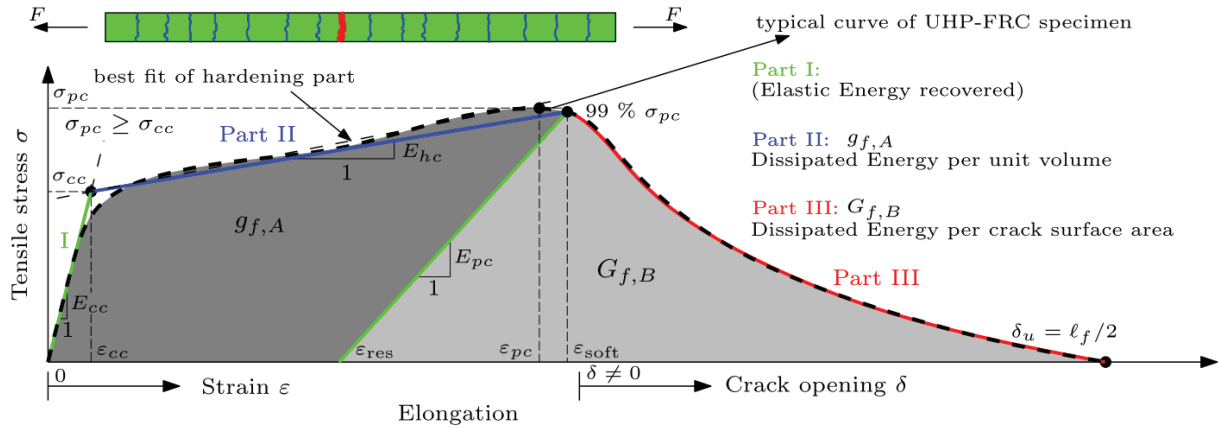


Figure 5 - Strain Hardening Tensile Behaviour of UHPFRC [18]

Fracture takes place when no more stress is transferred through the localised microcracks [11]. Unlike normal-strength concrete, UHPFRC possesses superior tensile and flexural strengths due to the strain hardening, facilitated by the presence of steel fibres. The volume fraction, type and aspect ratio of fibres in the matrix determine the exact tensile behaviour of UHPFRC.

Experimental results have been employed to formulate empirical equations, defining the CDP model for UHPFRC in tension (e.g., [11, 18]). However, previous experimental tensile stress-strain curves were used in this study to define the tensile behaviour of UHPFRC in ABAQUS using CDP model.

2.3 Modelling Full Scale RC and UHPFRC Beams

Prior to modelling UHPFRC retrofitted RC beams, the material models used for RC and UHPFRC need to be validated. For this purpose, a RC beam and a UHPFRC beam selected from previous experimental studies were separately modelled and their load-displacement curves were compared for numerical model validation. The study by Al-Osta et al. [19] was used in selecting the RC beam for modelling purposes. The control beam from the aforementioned study was numerically simulated for three-point bending using the material models mentioned in section 2.1. The geometry, reinforcement details, concrete grade and other details of the test beam can be found in the paper by Al-Osta et al. [19]. The CDP model for normal-strength concrete is well defined and thus, specific details of CDP in modelling the RC beam is not presented here. The analytically determined moment capacity of the RC control beam was 18.3 kNm whereas the experimental and

numerical moment capacities were 20.1 kNm and 18.9 kNm, respectively.

Once the normal-strength concrete beam was modelled, a full-scale UHPFRC beam was modelled, which was selected from the study by Singh et al. [15]. Figure 6 shows the geometry and the reinforcement details of the selected UHPFRC beam. Four (4) 16 mm diameter bars were used as longitudinal reinforcement in a 150 mm x 150 mm cross-section of the beam. The clear span of the beam was 1350 mm. 6 mm diameter shear links were used at 90 mm center-to-center spacing. The UHPFRC full-scale beam exhibited a compressive strength of 143 MPa and a tensile strength of 5.8 MPa, with a steel fiber content of 2.25% volume fraction. This beam was simply supported and subjected to a three-point bending test.

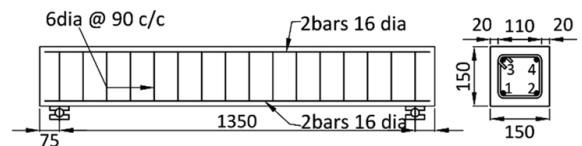


Figure 6 - Geometry and Reinforcement arrangement of Full Scale UHPFRC Beam [15]

The modified CDP model presented in section 2.2 was used in defining the material behaviour of UHPFRC. σ_{bo}/σ_{co} was defined as 1.05, k_c as 2/3, and the dilation angle φ as 30°. A fully bonded contact was modelled between the concrete and the reinforcement. Mesh size was set as 10 mm by performing preliminary mesh convergence studies to select the optimum mesh size minimising the computational time without compromising the accuracy of the results. Figure 7 shows the 3-D solid FE model of the beam and its mesh configuration.



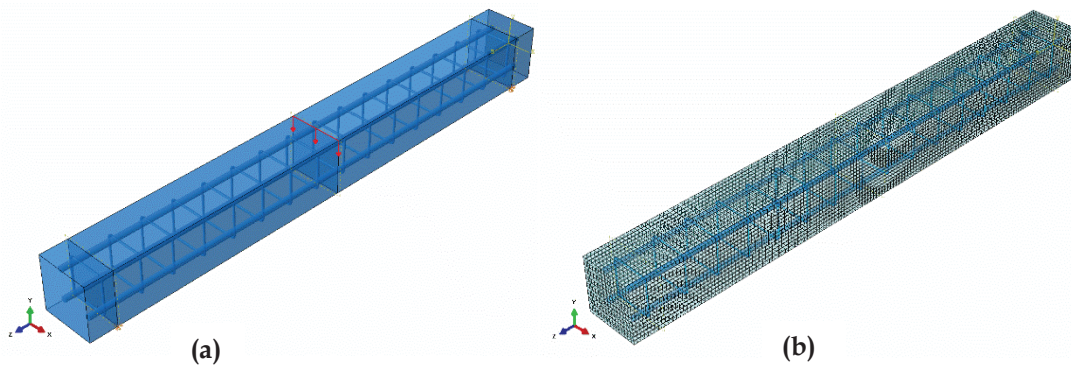


Figure 7 - UHPFRC Beam (a) 3-D Solid FE Model (b) Mesh Configuration

A displacement-controlled load was applied until the failure of the beam. This beam was with a higher span/depth ratio and a flexural failure was observed in the experimental results by initiating and propagating cracks at the mid-span of the beam where it is subjected to the highest bending moment [15]. Numerical model validation is presented in section 3 of this paper.

Once the model validation is completed, a parametric study was conducted by modelling a shear critical RC beam subjected to different UHPFRC jacketing configurations. The geometry and the reinforcement details of the selected control beam are shown in Figure 8. The shear span to depth ratio of this beam is 2, and a brittle shear failure was observed in this beam when subjected to a four-point bending test.

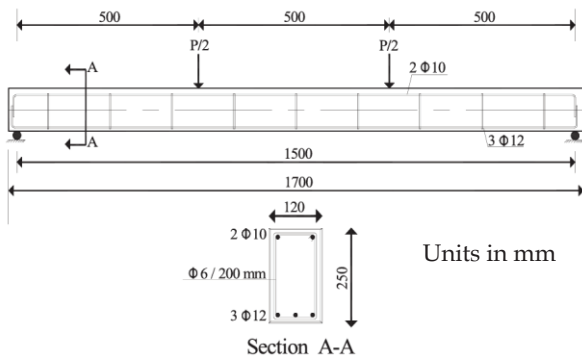


Figure 8 - Shear Critical Control Beam for the Parametric Study [3]

The effect of different UHPFRC retrofitting configurations on the behaviour of this control beam was studied by performing a parametric study. Figure 9 shows the 2-sided and 3-sided retrofitting configurations which were adopted for numerical simulation. Specimen B1 had a 25 mm 2-sided jacket thickness, whereas specimen B2 had a 35 mm 2-sided jacket thickness. A 3-sided jacketing configuration (U-jacket) was used in Specimen B3 as illustrated in Figure 9. Modeling the interface contact between the RC and UHPFRC is critical to obtaining the actual behavior of the retrofitted specimens. Typically,

when casting the jacket, the existing exterior surface of the RC beam is roughened by sandblasting or chipping to ensure a proper bond. Composite behaviour will only be guaranteed if the bonding is strong enough to eliminate debonding failure. Therefore, the interface can be either modelled as a bonded contact or a frictional contact. Further, advanced approaches like cohesive zone modelling can be adopted depending on the requirement [11]. The FE models incorporated a frictional contact by specifying the frictional coefficient. The coefficient of friction was used as 1.5 to represent a well-roughened interface. The value for friction coefficient used in this study (1.5) is very close to the value (1.4) recommended by the model code 2010 [20] for very well roughened interfaces.

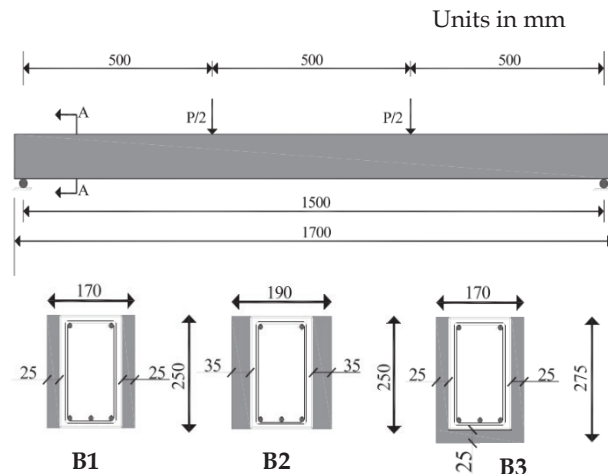


Figure 9 - Two-Sided and Three-Sided Jacketing along the Full Length of the RC Beam

Figure 10 illustrates the UHPFRC jacketing configuration only for the shear span of the shear critical beam. A 2-sided jacket of 25 mm thickness is applied to both the shear spans in the four-point bending arrangement. The 500 mm mid-span region of the RC beam is not retrofitted in Specimen B4.

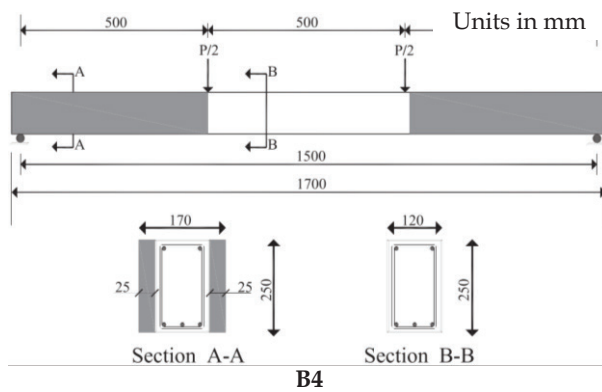


Figure 10 - Two-Sided Jacketing only for the Shear Span of the RC Beam

3. Results and Discussion

3.1 Numerical Model Validation - UHPFRC Beam Subjected to Three-Point Bending Test

Before conducting the parametric study, numerical model validation was carried out. UHPFRC beam subjected to three-point bending was analysed and the results were compared with the existing numerical results. Figure 11 shows some of the results from the FE model. The propagation of flexural cracks in the midspan of the beam is shown in Figure 11(a) and a flexural failure was observed in the beam. Figure 11(b) shows the yielding of the flexural reinforcement and the yield stress is 460 MPa, which was defined in the bilinear elastic-perfectly plastic behaviour of steel reinforcement. In this study, a beam subjected to flexural failure was used as the UHPFRC control beam in order to validate the model. However, it can be evidenced from the results of the previous studies that the use of Concrete Damage Plasticity (CDP) model in ABAQUS along with the modelling techniques used in this study can effectively capture the shear behaviour of beams subjected to bending tests (e.g., [21]). Further, previous researchers have used CDP model in ABAQUS to model the shear failure of other structural elements such as shear walls [11]. Therefore, the capability of the developed models in this study to capture the shear behaviour can be ensured.

Figure 12 illustrates the comparison of experimental and numerical load-displacement curves. The central deflection and the load applied to the beam were computed from the numerical model and plotted with the experimental values. A reasonable match between the experimental and numerical load-displacement curves can be observed in Figure 12. There is slightly a higher initial stiffness in the numerical model compared to

the experimental. The peak load in the numerical simulation was recorded as 113 kN at a central deflection of about 12 mm. Peak load in the experimental results was recorded as 110 kN at a central deflection of 19 mm. The ductile behaviour of the UHPFRC beam is noticeable in the load-displacement curve. Experimentally and numerically determined moment capacity of the UHPFRC control beam were 36.8 kNm and 39.2 kNm, respectively. Considering the initial stiffness, peak load, failure load, moment capacity and deflections at each of the critical loads, it can be concluded that the numerical model can reasonably simulate the behaviour of the UHPFRC beam via the employed CDP model.

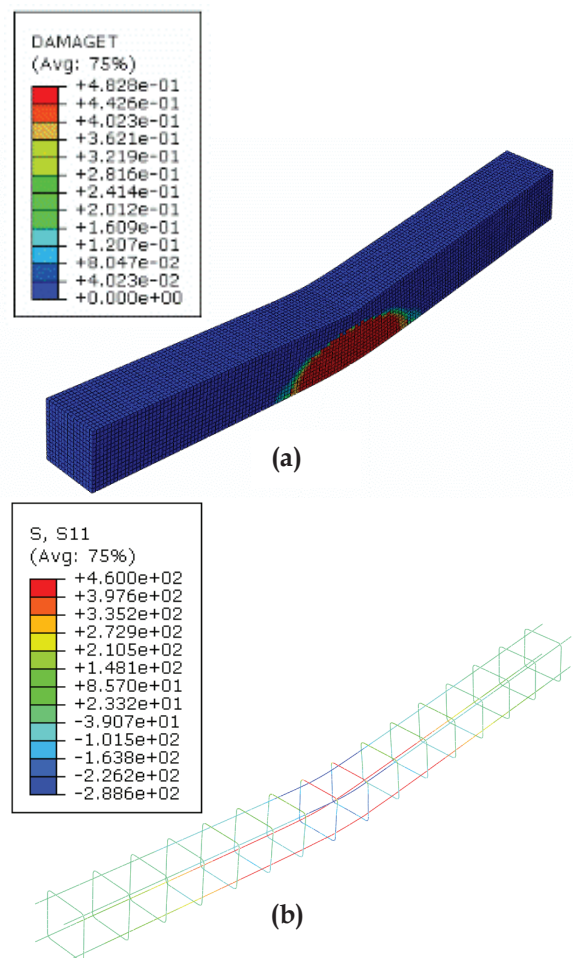


Figure 11 - UHPFRC Beam (a) Formation of Tensile Cracks (Tensile Damage) (b) Yielding of Tensile Reinforcement at the Mid-Span of the Beam

There can be potential possibilities for the slight variations observed in the experimental and numerical load-displacement curves. First reason can be modelling the UHPFRC as a homogeneous isotropic material in the numerical simulations. However, with the random distribution of steel fibres, there can be locations in the beam with fibre clogging which



can have local effects. Thus, the assumption of homogeneity in the numerical model can affect the comparison with experimental results. If the fibre distribution and local effects need to be captured, discrete element modelling is favoured over FE modelling.

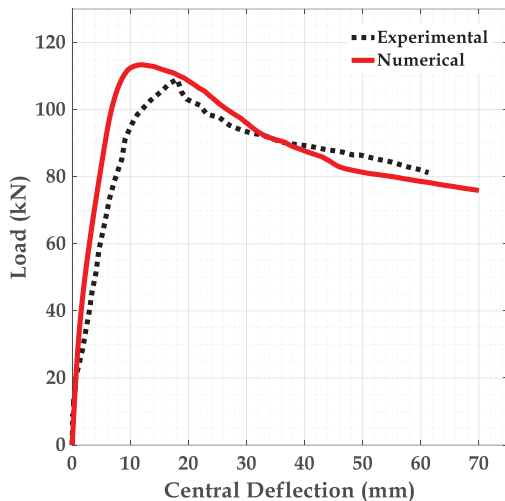


Figure 12 - Comparison of Experimental and Numerical Load-Displacement Curves

3.2 Parametric Study - UHPFRC Retrofitted RC Shear Critical Beams

For the control RC beam shown in Figure 8, a brittle shear failure was observed in the experimental results of Said et al. [3]. However, when this shear critical beam was retrofitted with UHPFRC jackets, a flexure failure by yielding longitudinal reinforcement was observed in the numerical simulations considering the four-point bending. Figure 13 shows the FE model of the 2-sided 25 mm UHPFRC jacketed RC beam. The flexure failure is noticeable from the flexural cracks observed in Figure 13(a) and the yielding of flexural reinforcement illustrated in Figure 13(b).

The findings indicate that retrofitting shear-critical beams with UHPFRC can effectively transform brittle shear failures into ductile flexure failures, thereby substantially improving the load-bearing capacity. Comparison of the load displacement curves of control beam, B1 and B2 specimens are shown in Figure 14. The calculated shear capacity of the RC control beam is 70.5 kN, while the experimentally obtained shear capacity is 66.5 kN. The control beam reaches a peak load of 133 kN with a central displacement of 12.5 mm, while the 25 mm 2-sided jacketed beam (specimen B1) achieves a peak load of 204 kN at a central deflection of 8.3 mm. This is a 53% increase in the peak load for the

UHPFRC retrofitted beam while reducing the central deflection at peak load by 34%.

In addition, the retrofitted beam exhibits a strong ductile behaviour compared to the control beam that failed in brittle shear. This behaviour is attributed to the resistance of the steel fibres in the UHPFRC matrix to initiate and propagate micro cracks. When the jacket thickness is increased to 35 mm (specimen B2), there is a further enhancement in the peak load. The peak load increases to 231 kN, reflecting a 74% increase compared to the control beam. Nevertheless, the central deflection at the point of failure remains relatively unchanged. Therefore, a greater jacket thickness contributes to an improved load-bearing capacity in UHPFRC-retrofitted shear-critical beams. However, it is important to consider the risk of debonding failure when opting for thicker jackets. Comparison of the load-displacement curves of 2-sided and 3-sided UHPFRC jacketed specimens are illustrated in Figure 15. For both scenarios, jacket thickness was modelled as 25 mm.

It is important to note that the effective depth of the 3-sided jacketed beam (specimen B3) increases to that of the control and 2-sided jacketed beam (specimen B1). The peak load for specimen B1 is 204 kN whereas that for specimen B3 is 255 kN. This peak load for specimen B3 is a 92% enhancement compared to the control beam. It is evident from this result that 3-sided jacketing performs far better than 2-sided jacketing with same jacket thickness for UHPFRC retrofitted shear critical RC beams. In contrast to 2-sided jacketing, the extreme fibers at the mid-span bottom, experiencing the highest bending stresses, consist of UHPFRC in 3-sided jacketing. This further enhances the flexural capacity of 3-sided jacketing in addition to the favourable effect from the increase in the effective depth.

Figure 16 shows the comparison of load-displacement curves for UHPFRC retrofitted shear critical beams for the full span (specimen B1) and only for the shear span (specimen B4). The failure modes of both cases were observed as ductile flexure failures as evident from the load-displacement curves in Figure 16. Specimen B4 shows a significantly higher ductility and higher initial stiffness compared to that of the control beam which failed in brittle shear. Nevertheless, there is no considerable enhancement in the load-carrying capacity.

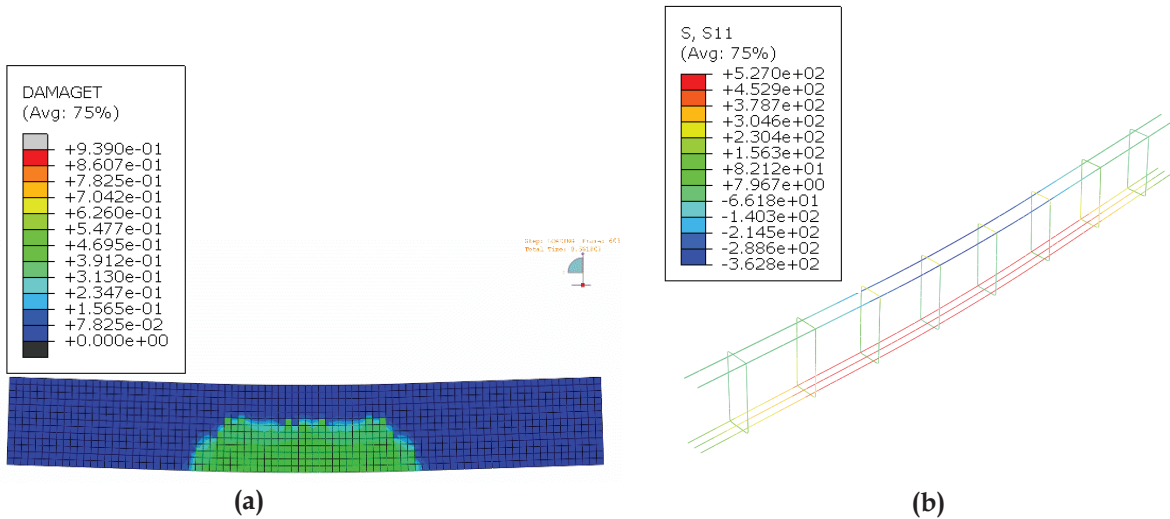


Figure 13 - UHPFRC Retrofitted RC Beam (a) Flexural Crack Propagation in the Mid-Span (b) Yielding of the Longitudinal Reinforcement

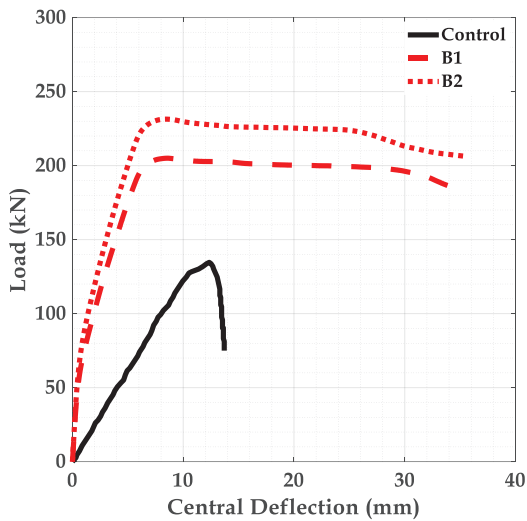


Figure 14 - Comparison of the Load Displacement Curves of Control, B1 and B2 Specimens

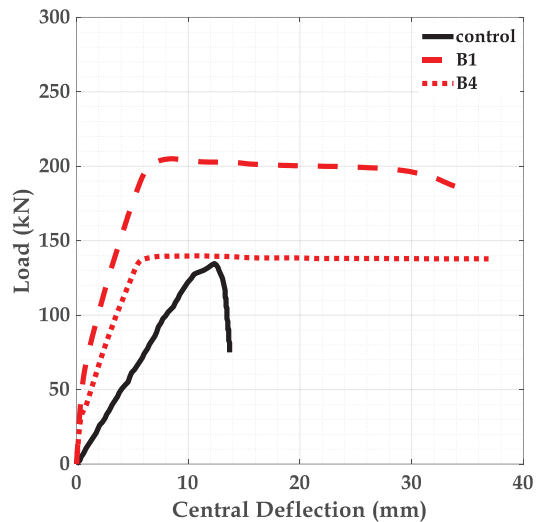


Figure 16 - Comparison of the Load Displacement Curves of Control, B1 and B4 Specimens

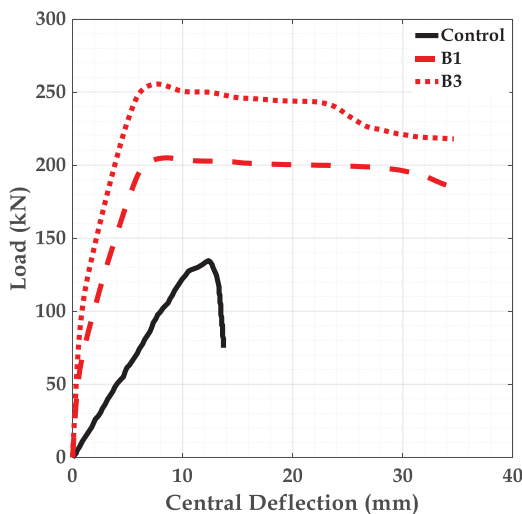


Figure 15 - Comparison of the Load Displacement Curves of Control, B1 and B3 Specimens

Due to UHPFRC jacketing, the shear failure mode is changed into flexure failure mode. When it is a flexure failure, the critical region is the midspan, and there is no support from UHPFRC in the midspan when only retrofitted in the shear span. This factor may explain the limited change in load-carrying capacity when only retrofitted for the shear span. From these results, it is evident that UHPFRC retrofitting only for the shear span is not that helpful in terms of the load-carrying capacity. Nevertheless, an initial improvement in stiffness and the attainment of ductile failure can be achieved by retrofitting only the shear span.



4. Conclusions

Numerical simulations via finite element analysis were performed in this study to investigate the effect of different UHPFRC jacketing configurations on the behaviour of RC shear critical beams. A modified CDP model was employed in simulating UHPFRC behaviour. Numerical model validation was carried out using existing experimental results. Finally, a parametric study was conducted to explore the effect of jacketing configuration on the performance of UHPFRC retrofitted shear critical RC beams. Based on the results obtained from the simulations, following conclusions can be drawn:

- Modified CDP model can effectively simulate the behaviour of UHPFRC retrofitted RC beams. This was evident from the comparison of numerical and experimental load-displacement curves.
- Load carrying capacity is increasing with the retrofitted UHPFRC jacket thickness. There is about 53% and 74% increase in load-carrying capacity for shear critical RC beams retrofitted with 2-sided UHPFRC using 25 mm and 35 mm jackets, respectively, compared to the control beam. However, it is important to take into account the risk of debonding failure when opting for thicker jackets. In addition, there is a significant enhancement of ductility in UHPFRC retrofitted beams.
- The load-carrying capacity of the 3-sided jacketed beam surpassed that of the 2-sided jacketed beam. The load-carrying capacity experiences an approximate increase of 92% for 3-side jacketed beams and 53% for 2-side jacketed beams compared to that of the control beam. Further, both jacketing configurations changed the failure mode of the control beam from brittle shear to ductile flexure. Substantial ductility enhancement was observed from the load displacement curves of UHPFRC retrofitted beams.
- Full-length jacketing significantly enhances the load-carrying capacity compared with the shear span jacketing. There is no substantial improvement in the load-carrying capacity for shear-critical RC beams retrofitted only in the shear span compared to the control beam. Retrofitting the shear span only enhances the ductility of the beam, not the strength, because of the change of the failure mode. Therefore, the overall behaviour must be considered when proposing a retrofitting methodology for

performance enhancement of structural elements.

Acknowledgement

Author wishes to acknowledge the assistance of undergraduate students from University of Peradeniya in performing the numerical simulations.

References

1. Akeed, M. H., Qaidi, S., Ahmed, H. U., Emad, W., Faraj, R. H., Mohammed, A. S., ... & Azevedo, A. R. (2022). Ultra-High-Performance Fiber-Reinforced Concrete. Part III: Fresh and hardened properties. *Case Studies in Construction Materials*, 17, e01265.
2. Akeed, M. H., Qaidi, S., Faraj, R. H., Majeed, S. S., Mohammed, A. S., Emad, W., ... & Azevedo, A. R. (2022). Ultra-High-Performance Fiber-Reinforced Concrete. Part V: Mixture Design, Preparation, Mixing, Casting, and Curing. *Case Studies in Construction Materials*, 17, e01363.
3. Said, A., Elsayed, M., Abd El-Azim, A., Althoey, F., & Tayeh, B. A. (2022). Using Ultra-High Performance Fiber Reinforced Concrete in Improvement Shear Strength of Reinforced Concrete Beams. *Case Studies in Construction Materials*, 16, e01009.
4. Camacho, E., López, J. Á., & Serna, P. (2012). Definition of Three Levels of Performance for UHPFRC-VHPFRC with available Materials. *Proceedings of Hipermat*, 249-256.
5. Akeed, M. H., Qaidi, S., Faraj, R. H., Mohammed, A. S., Emad, W., Tayeh, B. A., & Azevedo, A. R. (2022). Ultra-High-Performance Fiber-Reinforced Concrete. Part I: Developments, Principles, Raw Materials. *Case Studies in Construction Materials*, 17, e01290.
6. Bandara, S., Wijesundara, K., & Rajeev, P. (2023). Ultra-High-Performance Fibre-Reinforced Concrete for Rehabilitation and Strengthening of Concrete Structures: A Suitability Assessment. *Buildings*, 13(3), 614.
7. Marini, A., & Meda, A. (2009). Retrofitting of R/C Shear Walls by Means of High-Performance Jackets. *Engineering Structures*, 31(12), 3059-3064.
8. Altin, S., Koprman, Y., & Baran, M. (2013). Strengthening of RC Walls using Externally Bonding of Steel Strips. *Engineering Structures*, 49, 686-695.

9. Dan, D. (2012). Experimental Tests on Seismically Damaged Composite Steel Concrete Walls Retrofitted with CFRP Composites. *Engineering Structures*, 45, 338-348.
10. Chikh, A., Tounsi, A., Hebali, H., & Mahmoud, S. R. (2017). Thermal Buckling Analysis of Cross-Ply Laminated Plates using a Simplified HSDT. *Smart Structures and Systems*, 19(3), 289-297.
11. Sakr, M. A., El-khoriby, S. R., Khalifa, T. M., & Nagib, M. T. (2019). Modeling of RC Shear Walls Strengthened with Ultra-High Performance Fiber Reinforced Concrete (UHPFRC) Jackets. *Engineering Structures*, 200, 109696.
12. Habel, K., Denarié, E., & Brühwiler, E. (2006). Structural Response of Elements Combining Ultrahigh-Performance Fiber-Reinforced Concretes and Reinforced Concrete. *Journal of Structural Engineering*, 132(11), 1793-1800.
13. Safdar, M., Matsumoto, T., & Kakuma, K. (2016). Flexural Behavior of Reinforced Concrete Beams Repaired with Ultra-High Performance Fiber Reinforced Concrete (UHPFRC). *Composite Structures*, 157, 448-460.
14. Lubliner, J., Oliver, J., Oller, S., & Onate, E. (1989). A Plastic-Damage Model for Concrete. *International Journal of Solids and Structures*, 25(3), 299-326.
15. Singh, M., Sheikh, A. H., Ali, M. M., Visintin, P., & Griffith, M. C. (2017). Experimental and Numerical Study of the Flexural Behaviour of Ultra-High-Performance Fibre Reinforced Concrete Beams. *Construction and Building Materials*, 138, 12-25.
16. Kurihara, N., Kunieda, M., Kamada, T., Uchida, Y., & Rokugo, K. (2000). Tension Softening Diagrams and Evaluation of Properties of Steel Fiber Reinforced Concrete. *Engineering Fracture Mechanics*, 65(2-3), 235-245.
17. Graybeal, B. A. (2007). Compressive Behavior of Ultra-High-Performance Fiber-Reinforced Concrete. *ACI Materials Journal*, 104(2), 146.
18. Wille, K., El-Tawil, S., & Naaman, A. E. (2014). Properties of Strain Hardening Ultra High-Performance Fiber Reinforced Concrete (UHP-FRC) Under Direct Tensile Loading. *Cement and Concrete Composites*, 48, 53-66.
19. Al-Osta, M. A., Isa, M. N., Baluch, M. H., & Rahman, M. K. (2017). Flexural Behavior of Reinforced Concrete Beams Strengthened with Ultra-High Performance Fiber Reinforced Concrete. *Construction and Building Materials*, 134, 279-296.
20. CEB-FIP (Comité Euro International du Béton; Fédération International de la Précontraint). *Fib Bulletin 55: Model Code 2010, Vol. 1. Lausanne: International Federation for Structural Concrete (fib); 2010.*
21. Mansour, W., & Tayeh, B. A. (2020). Shear Behaviour of RC Beams Strengthened by Various Ultrahigh Performance Fibre-Reinforced Concrete Systems. *Advances in Civil Engineering*, 2020, 1-18.

